Dynamic hysteresis curves in a mixed spin ternary alloy system under the time-dependent magnetic field

Article *in* Physica Scripta · August 2023

DOI: 10.1088/1402-4896/acf005

CITATIONS
0

READS
46

2 authors:

Mehmet Ertaş
Erciyes Üniversitesi
88 PUBLICATIONS **1,356** CITATIONS

SEE PROFILE

Mehmet Bati
Recep Tayyip Erdoğan Üniversitesi
29 PUBLICATIONS **162** CITATIONS

SEE PROFILE

PAPER

Dynamic hysteresis curves in a mixed spin ternary alloy system under the time-dependent magnetic field

To cite this article: M Ertaş and M Batı 2023 *Phys. Scr.* **98** 095944

Physica Scripta

PAPER

Dynamic hysteresis curves in a mixed spin ternary alloy system under the time-dependent magnetic field

RECEIVED
28 May 2023

REVISED
17 July 2023

ACCEPTED FOR PUBLICATION
14 August 2023

PUBLISHED
24 August 2023

M Ertaş[1] and M Batı[2]

[1] Physics Department, Erciyes University, 38039 Kayseri, Turkey
[2] Physics Department, Recep Tayyip Erdoğan University, 53100 Rize, Turkey

E-mail: mehmet.bati@erdogan.edu.tr

Keywords: hysteresis, mixed spin, ternary alloys, phase transitions, dynamic phenomena

Abstract

The dynamic hysteresis features in mixed spins-$(1/2,\ 3/2,\ 5/2)$ ternary alloy system with formula $AB_pC_{(1-p)}$ was examined through Glauber-type stochastic dynamic and mean-field theory. The system includes two interpenetrating lattices, one has spin-$1/2$ components, while the other includes a random distribution of spin-$3/2$ and spin-$5/2$ compounds. The effect of Hamiltonian parameters on the dynamic hysteresis behavior was investigated in detail and observed that the physical characteristics have a significant impact on the shape and quantity of hysteresis loops. We compared our findings with other theoretical and experimental investigations; a high level of agreement is obtained.

1. Introduction

Molecule-based magnets display striking characteristics, namely inverted magnetic hysteresis loop, multi-compensation behavior, and photo-induced magnetization. Including spintronics, information quantum computing, molecular electronics, and storage, molecule-based magnets have shown promise for a variety of uses [1–5]. Prussian Blue Analogs (*PBA*) which is a type of molecular magnet, has been widely explored in the previous decade due to the ability to adjust their compositional concentration during synthesis and the effect that this manipulation has on the system's magnetic features. *PBA* has been theoretically modeled as ternary metallic alloys having the formula $AB_pC_{(1-p)}$. As far as spin sizes are concerned, the equilibrium features of the mixed-spin ternary alloy system built of a great variety of combinations of the spin magnitudes have been investigated using Green's functions, Bethe approximation, Monte Carlo simulations, effective field theory, mean field theory, among others (see [6–11] and therein).

Despite the extensive literature on equilibrium magnetic properties of the systems, to our best knowledge, there are only several studies on the ternary alloy system's dynamic characteristics [12–17]. Overall, magnetic ternary alloy dynamic phenomena are complicated and diverse, and understanding them is essential for designing and refining these materials for a variety of technological applications, such as magnetic storage, sensing, and energy conversion. To fully understand the complex magnetic behavior of ternary alloys and discover their potential for cutting-edge and new applications, more theoretical investigation and experimentation are required. When a magnetically interacting, system is driven by a time-dependent magnetic field varying sinusoidally, the system may not respond to the external field simultaneously. Owing to the existence of a competition between the system's relaxation behavior and the period of the driving field, one important striking phenomenon which has important technological applications and intriguing physics occurs, dynamic hysteresis behavior, namely the hysteretic response of the kinetic Ising system to the periodically oscillating magnetic fields. Scientists are currently focused on the nonequilibrium system behavior. The dynamic phase lag between the instantaneous magnetization and the periodic external magnetic field is connected to the hysteresis phenomena. In contrast to the results observed in equilibrium systems in which the magnitude of the external field does not explicitly change with time, dynamic hysteresis in a non-equilibrium system is observed in the paramagnetic phase. In other words, a ferromagnetic material has nonzero coercivity in the presence of

static magnetic fields. In the proximity of the ferromagnetic paramagnetic phase transition zone, this coercive field drops to zero with the use of the Hamiltonian parameter as an adjustable parameter, such as raising the temperature, frequency, crystal field, etc. The relaxation time of the system at high oscillation frequencies of the external field is relatively much larger than the oscillation period of the external perturbation. As a result of the system's inability to follow the driving field, dynamic symmetry is lost, resulting in asymmetric hysteresis curves. Because magnetization never reaches zero, coercivity is irrelevant in this case. The system approaches the dynamic paramagnetic phase as the field frequency decreases or the external field's amplitude rises, and symmetric hysteresis loops with nonzero coercivity are seen [18–22]. The most well-known kinetic Ising-type hysteresis curve takes the shape of a Lissajous curve and is caused by the fluctuation of time-dependent magnetization $m(t)$ with an external field $h(t)$. This widespread phenomenon has gotten a lot of attention because of its vast range of potential applications. Dynamic hysteresis behaviors can be observed experimentally in various materials and systems, such as $NiFe/Cu/Co(001)$ spin-valve structures, epitaxial single ferromagnetic $fcc\ NiFe(001)$, permalloy thin films, magnetic $[Co/Pt]_3$ multilayers, the ternary intermetallic compound, $Pb_{0.4}Sr_{0.6}TiO_3$ ferroelectrics film, single crystalline compound $Co_7(TeO_3)_4Br_6$, etc [23–27]. Moreover, theoretically, dynamic hysteresis behaviors have been explored mostly using three models: (i) The time-dependent Landau–Lifshitz-Gilbert equations (ii) Extended domain wall models (iii) Ising kind systems such as one or mixed spin systems (see [28–35] references therein).

In conclusion, this manuscript presents a comprehensive study of the dynamic magnetic hysteresis properties of ternary alloys, highlighting the effect of Hamiltonian parameters. To achieve this goal, an $AB_pC_{(1-p)}$ ternary alloy system consisting of spins $S_i^A = 1/2$, $S_j^B = 3/2$, and $S_j^C = 5/2$ was simulated using a Glauber-type stochastic dynamic using the mean-field approximation. On the other hand, three characteristics can determine the dynamic hysteresis loops' shape; namely dynamic hysteresis loop area, coercivity field, and remanent magnetization. In magnetic recording media, these characteristics are crucial [36]. Real tests of the quality of magnetic recording medium and their connection to hysteresis-based approaches can be found in [37]. Therefore, the understanding of the dynamic magnetic hysteresis properties of ternary alloys is crucial for their utilization in various technological applications, and this work aims to provide valuable insights and directions for further research in this field.

Eventually, for these purposes, the paper's outline is as follows: In section 2 we introduce the model and formulations. The numerical results and discussion are presented in section 3. Finally, section 4 presents a summary of our conclusions.

2. Model and formulation

We can describe a ferro–ferrimagnetic Ising ternary alloy' spin Hamiltonian as follows:

$$\begin{aligned}\mathscr{H} &= -J_{AB}\sum_{\langle ij\rangle} S_i^A S_j^B \varepsilon_j - J_{AC}\sum_{ij} S_i^A S_j^C (1-\varepsilon_j) \\ &- D\sum_j (S_j^B)^2 \varepsilon_j - D\sum_j (S_j^C)^2 (1-\varepsilon_j) \\ &-H(t)\sum_i S_i^A + H(t)\sum_j S_j^B \varepsilon_j + H(t)\sum_j S_j^C (1-\varepsilon_j).\end{aligned} \tag{1}$$

A time-dependent oscillating magnetic field is identified as $H(t) = H_0\cos(\omega t)$ that t, ω, and H_0 are the time, angular frequency, and amplitude. The D is the crystal field. $J_{AB} > 0$ and J_{AC} are the exchange interaction parameters between the nearest-neighbor magnetic particles. ε_j is a distributed random variable with a value of one or zero depending on whether site j is occupied by an ion of B or C and it can be described as $P(\varepsilon_j) = p\delta(\varepsilon_j - 1) + (1-p)\delta(\varepsilon_j)$. While the p is the concentration of B ion, $(1-p)$ is the concentration of C ion. The evolves according to the Glauber-type stochastic process at a rate of $1/\tau$. Glauber-type stochastic dynamics is applied to obtain the system's dynamical equations. If the S_i^A—and S_j^B – spins remain constant for a moment, the master equation for S_j^C– spins are stated as

$$\begin{aligned}&\frac{d}{dt}P(S_1^C, S_2^C, \ldots, S_N^C; t) \\ &= -\sum_j \left(\sum_{S_j^C \neq S_j^{C'}} W(S_j^C \to S_j^{C'}) \right) P(S_1^C, S_2^C, \ldots, S_j^C, \ldots, S_N^C) \\ &+ \sum_j \left(\sum_{S_j^C \neq S_j^{C'}} W(S_j^{C'} \to S_j^C) \right) P(S_1^C, S_2^C, \ldots, S_j^{C'}, \ldots, S_N^C)\end{aligned} \tag{2}$$

$W(S_j^C \rightarrow S_j^{C'})$ is the probability per unit of time that the j th spin changes from a value S_j^C to $S_j^{C'}$. With the probability per unit of time, each spin can change from the value S_j^C to $S_j^{C'}$,

$$W(S_j^C \rightarrow S_j^{C'}) = \frac{1}{\tau} \frac{\exp\left(-\frac{1}{k_B T_A}\Delta E(S_j^C \rightarrow S_j^{C'})\right)}{\sum_{\sigma_i'} \exp\left(-\frac{1}{k_B \ T_A}\Delta E(S_j^C \rightarrow S_j^{C'})\right)}. \tag{3}$$

k_B is the Boltzmann factor. T_A is described as absolute temperature and $\sum_{S_j^{C'}}$ is the sum of the five possible values of $S_j^{C'} = \mp\frac{5}{2}, \mp\frac{5}{2}, \mp\frac{1}{2}$. When equations (1)–(3) are combined with the mean-field theory, the dynamic equation for S_j^C-spins are shown to be as follows.

$$\Omega\frac{dm_C}{d\xi} = -m_C + \frac{5e^{\frac{2d(1-p)}{k_B T_A}}\sinh\left[\frac{5}{2\ k_B T_A}x\right] + 3e^{-\frac{2d(1-p)}{k_B T_A}}\sinh\left[\frac{3}{2\ k_B T_A}x\right] + e^{-4\frac{d(1-p)}{k_B T_A}}\sinh\left[\frac{1}{2\ k_B T_A}x\right]}{2e^{\frac{2d(1-p)}{k_B T_A}}\cosh\left[\frac{5}{2\ k_B T_A}x\right] + 2e^{-\frac{2d(1-p)}{k_B T_A}}\cosh\left[\frac{3}{2\ k_B T_A}x\right] + 2e^{-4\frac{d(1-p)}{k_B T_A}}\cosh\left[\frac{1}{2\ k_B T_A}x\right]}. \tag{4a}$$

Where $x = J_{AC} z_{AC} m_A(1-p) + H_0\cos(\xi)(1-p)$, $\xi = wt$, $S_j^C \equiv m_C$, $\Omega = \tau w$, $z_{AC} = 3$. Similarly, dynamic equations for S_j^B- and S_i^A- spins are shown to be as follows.

$$\Omega\frac{dm_B}{d\xi} = -m_B + \frac{3\sinh\left[\frac{3}{2\ k_B T_A}(J_{AB} m_A z_{BA} p + H_0\cos(\xi)p)\right] + e^{-2\frac{d}{k_B T_A}}\sinh\left[\frac{1}{2\ k_B T_A}(J_{AB} m_A z_{BA} p + H_0\cos(\xi)p)\right]}{2\cosh\left[\frac{3}{2\ k_B T_A}(J_{AB} m_A z_{BA} p + H_0\cos(\xi)p)\right] + 2e^{-2\frac{d}{k_B T_A}}\cosh\left[\frac{1}{2\ k_B T_A}(J_{AB} m_A z_{BA} p + H_0\cos(\xi)p)\right]}, \tag{4b}$$

$$\Omega\frac{dm_A}{d\xi} = -m_A + \frac{1}{2}\tanh\left[\frac{1}{2\ k_B T_A}(J_{AB} m_B z_{AB} p + J_{AC} m_C z_{AC}(1-p) + H_0\cos(\xi))\right], \tag{4c}$$

where $S_j^B \equiv m_B$, $S_i^A \equiv m_A$, $z_{AB} = z_{AC} = z_{BA} = z_{CA} = 3$. The physical parameters have been scaled by $J_{AB} = 1.0$. Physical quantities are defined as $T = \frac{k_B T_A}{J_{AB}}$, $d = \frac{D}{J_{AB}}$ and $h_0 = \frac{H_0}{J_{AB}}$, throughout the paper, respectively. The dynamic order parameters,

$$M_i = \frac{1}{2\pi}\int_0^{2\pi} m_i(\xi)d\xi \tag{5}$$

where $i = A,\ B$, and C. We can define the dynamic hysteresis loop area as follows,

$$A = \oint m(t)dh = -h_0\omega \oint m(t)\cos(\omega t)dt, \tag{6}$$

Solution and discussion of the equations will be given in the next section.

3. Numerical results and discussion

The equations (4)–(6) are solved with numerical methods such as Adams-Moulton-predictor-corrector with the Romberg integration and illustrated in figures 1–9. It is worth emphasizing that because of the domains present in ferromagnetic materials, the variation M versus h is non-linear. A full discussion of the formation of the hysteresis loop (HL) and the properties of domains may be found in, e.g. [38]. The form of the HL can be governed by three properties: HL area, *CF*, and *RM*. The HL area, also known as hysteresis loss or magnetic energy loss, is a measure of the energy loss per unit volume of the material. Designing effective magnetic devices, such as transformers, inductors, and electric motors, requires an understanding of the HL area. By minimizing energy waste, lowering hysteresis loss increases these devices' efficiency. To obtain smaller hysteresis loop regions and more energy-efficient systems, engineers and scientists evaluate and improve materials. The *CF*' physical significance lies in its connection to the stability of magnetization in a material. Materials with a higher coercive field are more resistant to demagnetization, meaning they can retain their magnetization even in the presence of strong external magnetic fields. This property is crucial for applications that require stable and long-lasting magnets, such as electric motors, magnetic sensors and in hard disk drives. The physical relevance of *RM* is seen in its link to a material's magnetic characteristics. Higher remanent magnetization materials can retain a considerable magnetic field after the external field is withdrawn, showing a strong 'memory' of their magnetization state. This feature is significant in permanent magnets and magnetic storage systems because it enables the development of long-term magnetic fields or the storing of data. The anisotropy of magnetism is primarily responsible for the varied shapes observed in the hysteresis loop for ferromagnetic materials. The shape depends also on the different physical conditions, e.g., T, J_{AC}, p, ω.

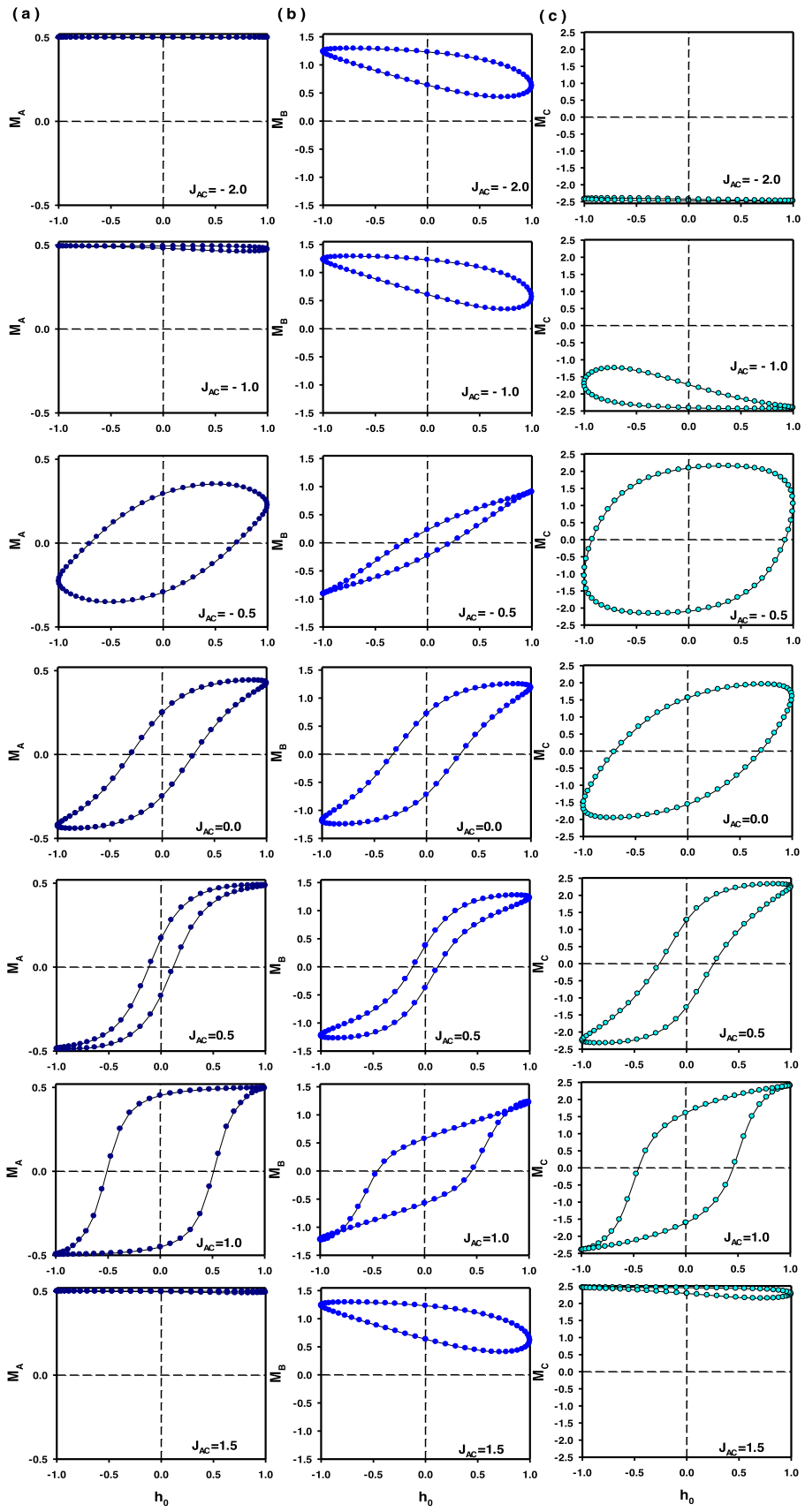

Figure 1. The dynamic magnetic hysteresis loops of the system with varying J_{AC} from −2.0 to 1.5 at $T = 1.0$, $d = 1.0$, $h_0 = 1.0$, $\omega = 0.06\pi$, and $p = 0.5$ (a) M_A (b) M_B and (c) M_C.

The dynamic HL area is calculated for varying J_{AC} from −2.0 to 1.5 and seen in figures 1(a)–1(c). This figure shows that the dynamic HL area increases up to a certain value of J_{AC} and then decreases. The HL illustrates symmetrical behavior for $-0.53 \leqslant J_{AC} < 1.20$. The triple hysteresis behavior is observed in the HL of the system

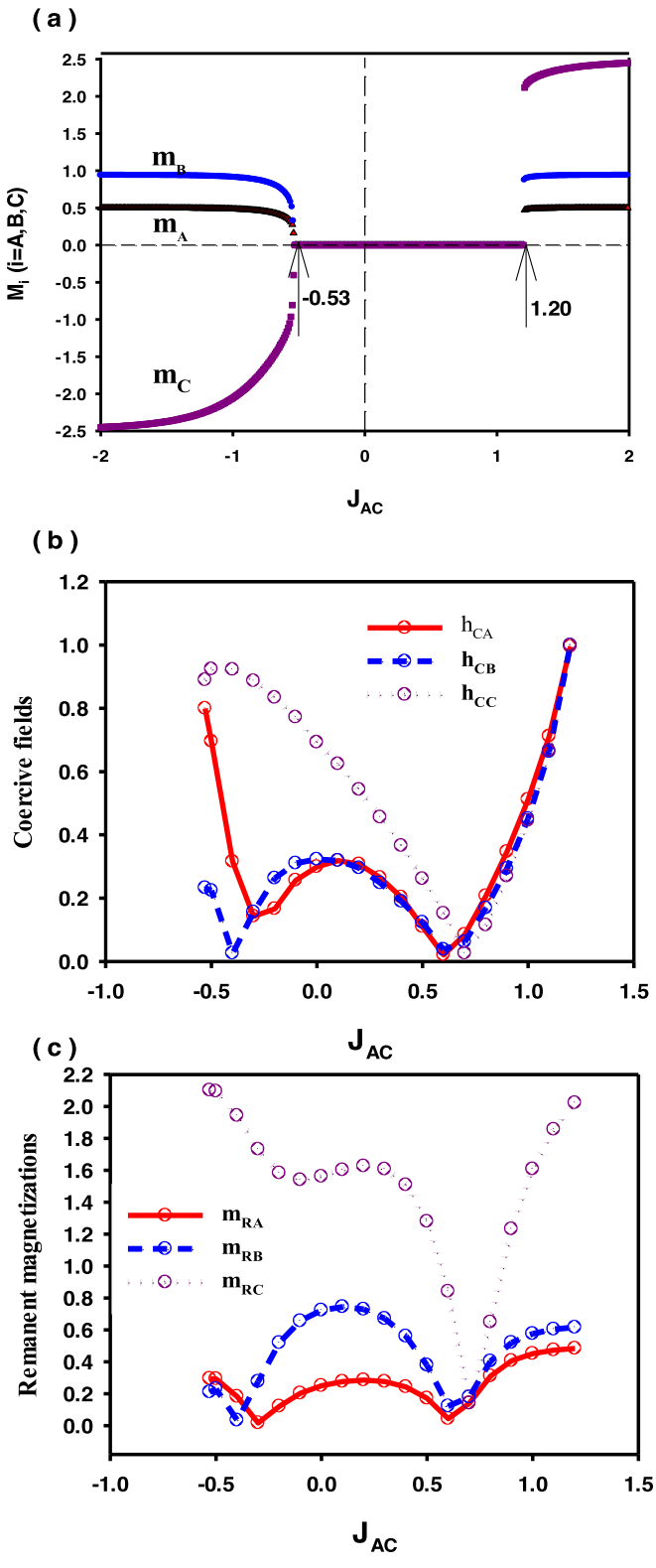

Figure 2. Magnetizations, Coercive field, and Remanent magnetizations versus J_{AC} with same parameter in figure 1.

at $0.64 < J_{AC} < 1.00$ values. The dynamic order parameter, namely dynamic magnetization (M), coercivities field (CF), and remanent magnetization (RM)' temperature-dependent behaviors are shown in figure 2(a)-(c), respectively. Figure 2(a) is observed that the system undergoes the first-order phase transitions from the ferrimagnetic phase to the paramagnetic phase at $J_{AC} = -0.53$ and $J_{AC} = 1.20$. It is seen from figure 1 and figure 2(a) that the system shows symmetrical behavior in the paramagnetic phase and asymmetrical in the ferrimagnetic phase. Figure 2(b) illustrates that h_{CA} and h_{CB} coercivities fields first decrease with the increase in J_{AC}, then increase, and continue their movement in this way and finish by increasing last. On the other hand, h_{CC}

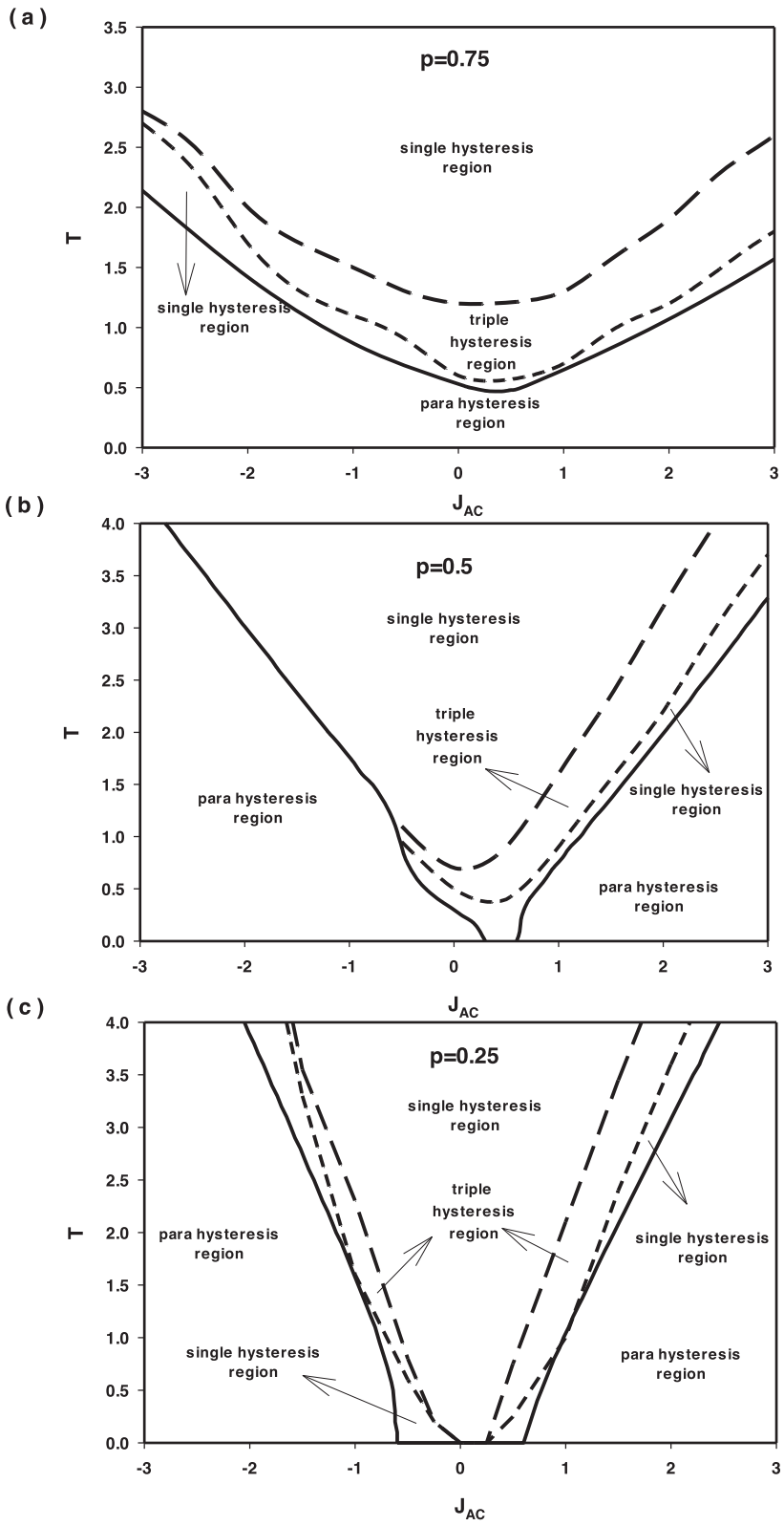

Figure 3. The hysteresis region in ($J_{AC} - T$) plane for $p = 0.75$, 0.5 and 0.25.

coercivity field first increases with the increase in J_{AC}, then decrease and finishes by increasing last. The *RM* in figure 2(c) shows similar behavior to the *CF* in figure 2(b). The hysteresis region in the $J_{AC} - T$ plane for $p = 0.75,\ 0.5$ and 0.25 plotted are in figures 3(a)–(c), for $d = 1.0$, $h_0 = 1.0$, $\omega = 0.06\pi$. It is seen that the triple hysteresis region is wider at $p = 0.75$ and narrows as p decreases. For $p = 0.5$, triple hysteresis is not observed at $J_{AC} < -0.5$ values. We examine the crystal-field interactions' effect on the HL for a large selection of d, namely $-3.0 \leqslant d \leqslant 3.0$ in figure 4 and the system shows the elliptical HL shape for high negative values of d. To understand the physical mechanism behind the effect of the d on hysteresis loop quantities, we need to consider

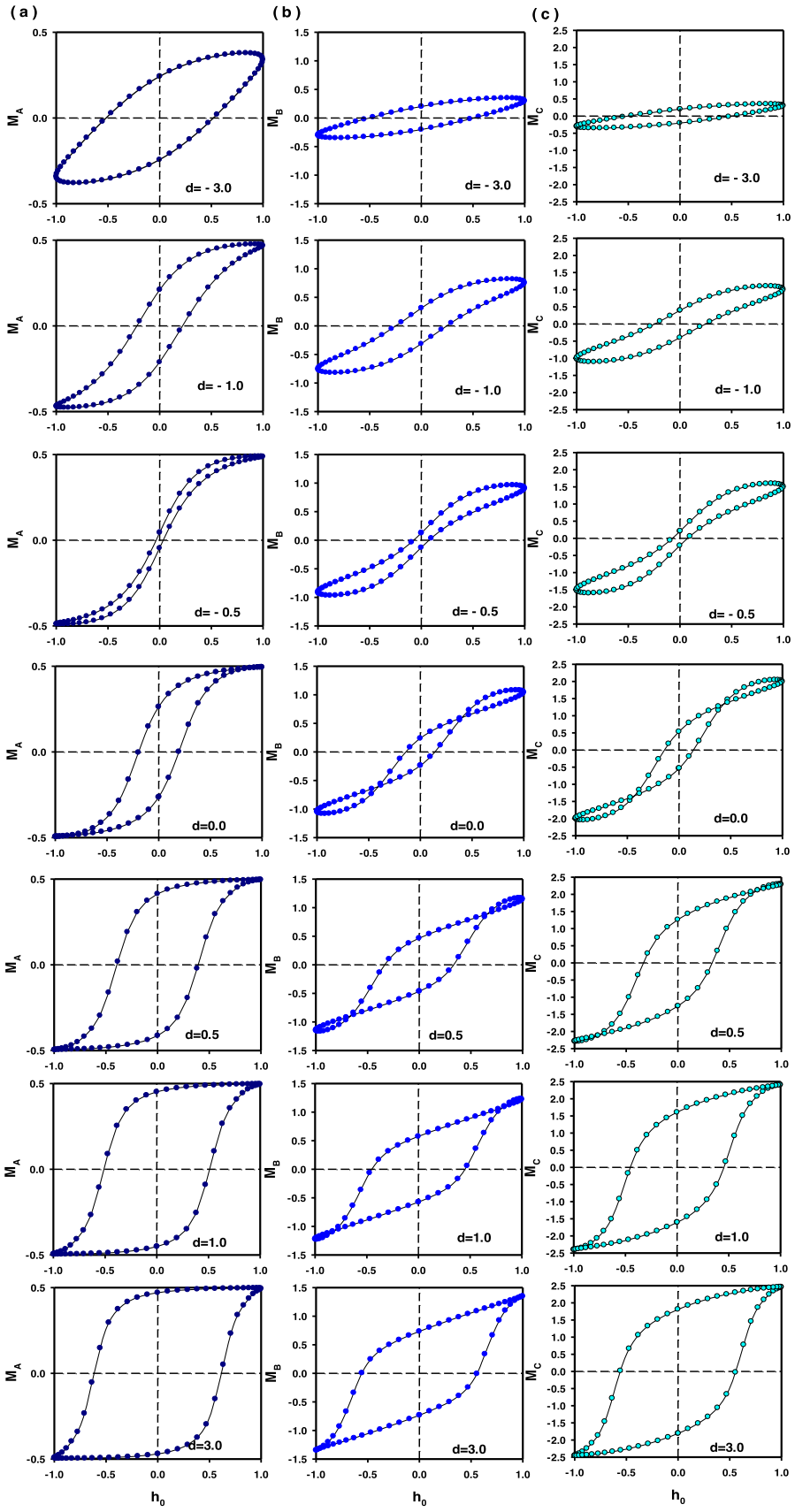

Figure 4. The dynamic magnetic hysteresis loops of system with varying d from -3.0 to 3.0 at $T = 1.0$, $J_{AC} = 1.0$, $h_0 = 1.0$, $\omega = 0.06\pi$, and $p = 0.5$ (a) M_A (b) M_B and (c) M_C.

the interaction between the crystal field and the magnetic moments of the material. The asymmetry of the charge distribution surrounding each magnetic ion is what causes this interaction to occur. The energy barrier that must be crossed for the magnetic moments to change direction can be affected by the crystal field, which in turn

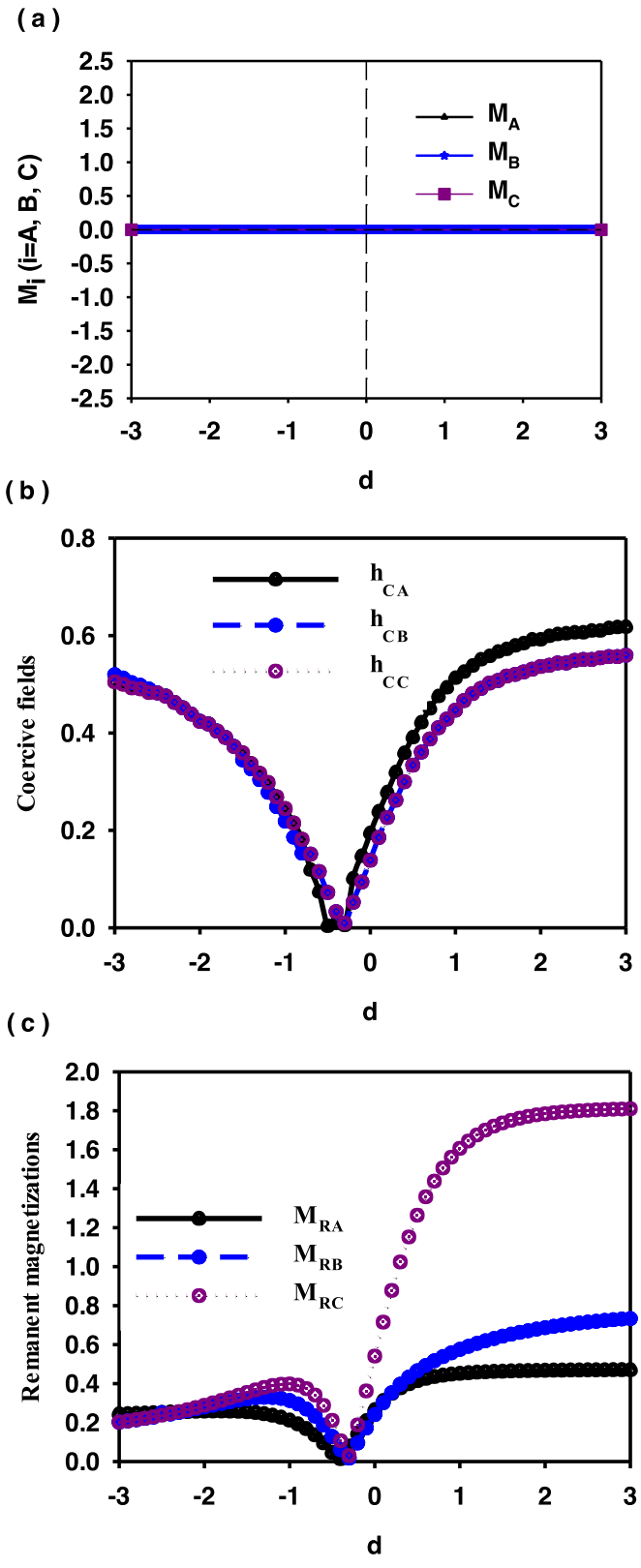

Figure 5. Magnetizations, Coercive field, and Remanent magnetizations versus d with same parameter in figure 4.

can impact the coercive field. By altering the stability of the magnetic domains within the substance, the crystal field can have an impact on the remanent magnetization. A crystal field's influence on certain magnetization directions can determine the magnetic moments' preferred orientation. As a result, even in the absence of an external magnetic field, the material may maintain a higher remanent magnetization. With increasing d, the type of HL changes from single to triple loops. Single hysteresis usually refers to a straightforward lagging effect, where the system's current state is only dependent on its recent history. This phenomenon is frequently seen in

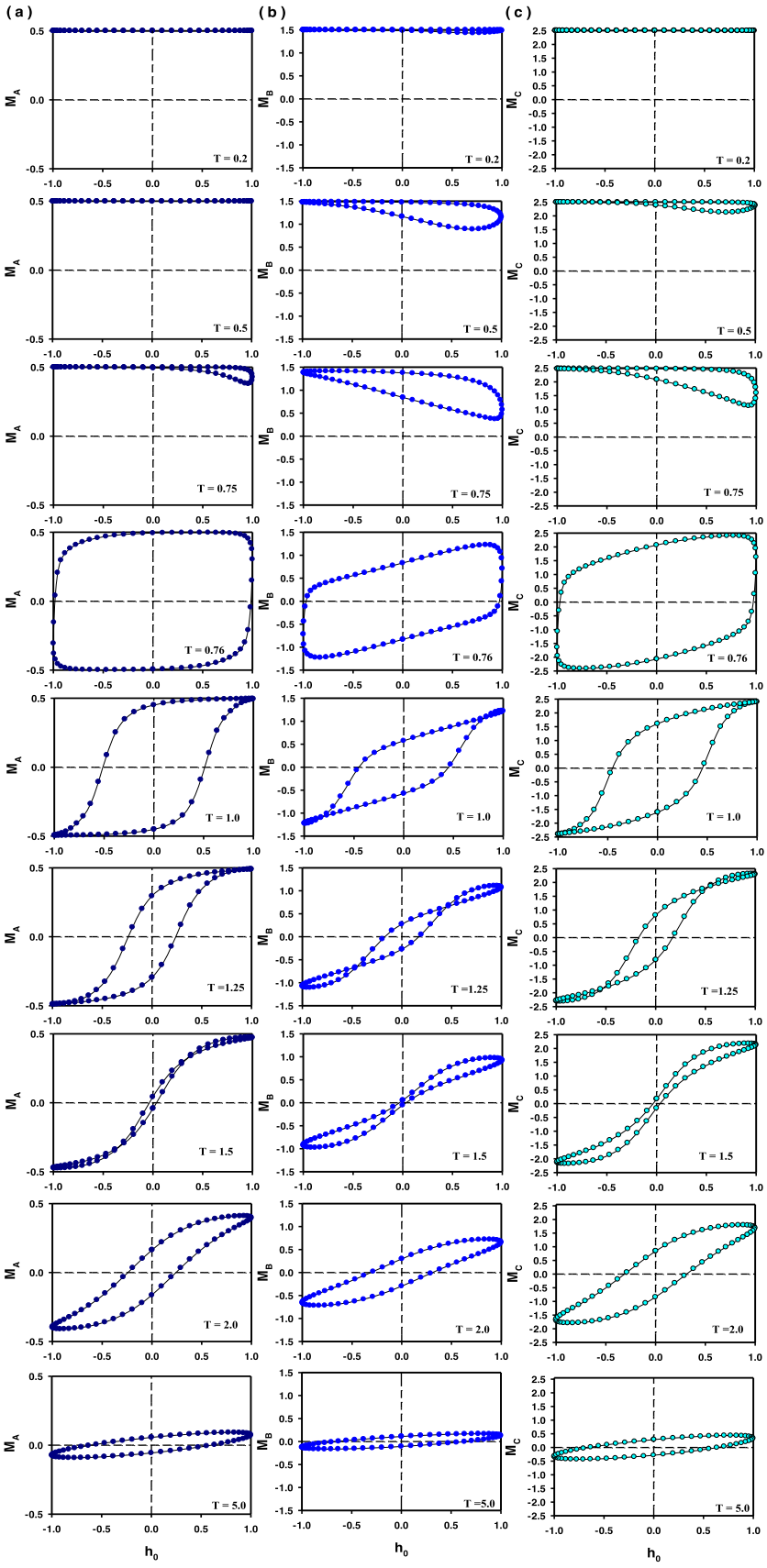

Figure 6. The dynamic magnetic hysteresis loops of the system with varying T from 0.2 to 5.0 at $J_{AC} = 1.0$, $d = 1.0$, $h_0 = 1.0$, $\omega = 0.06\pi$, and $p = 0.5$ (a) M_A (b) M_B and (c) M_C.

memory-rich systems, including ferromagnetic materials or certain mechanical systems. In contrast, triple hysteresis behavior shows a more sophisticated trailing effect, where the system's reaction is influenced by both recent and distant history in addition to its immediate past. Systems with large nonlinearities or long-term

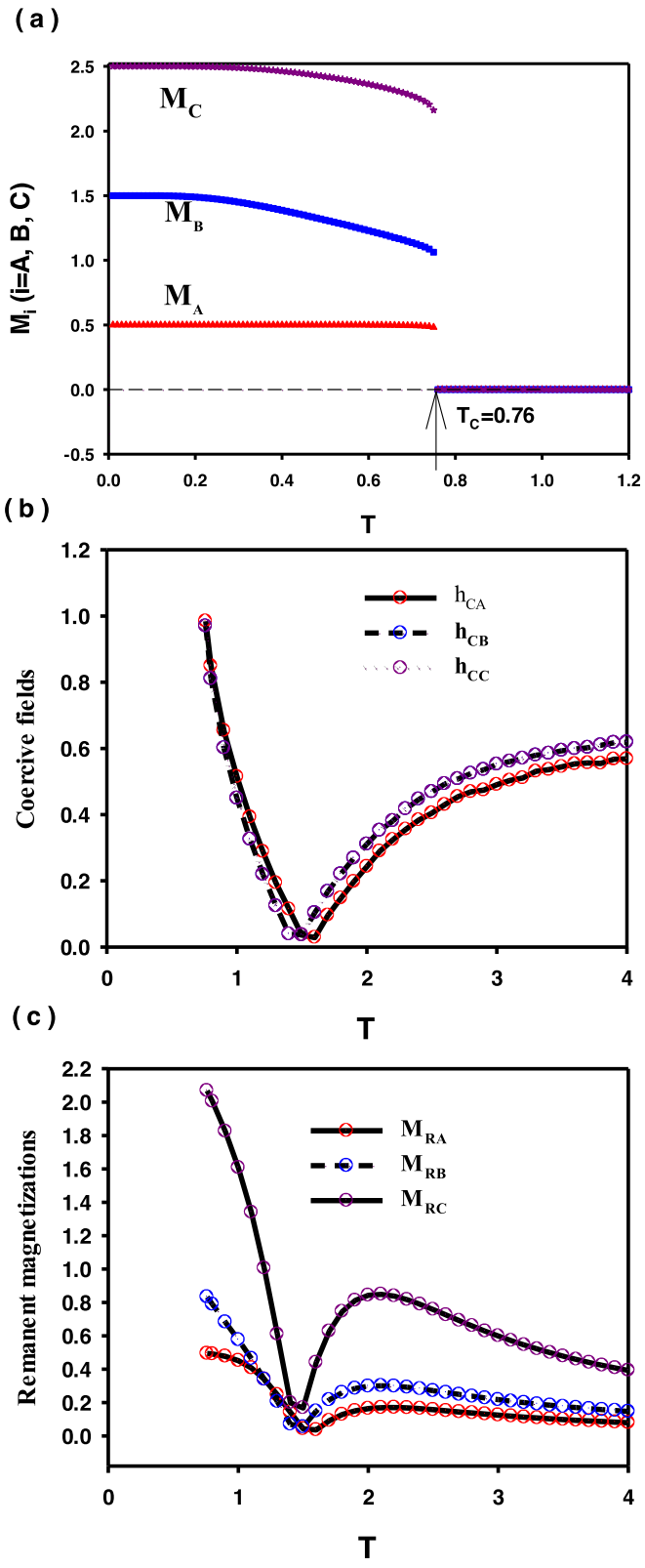

Figure 7. Magnetizations, Coercive field, and Remanent magnetizations versus T with same parameter in figure 7.

memory frequently exhibit this behavior. HL takes the shape of a Lissajous curve for high positive values of d. These results are in a good agreement with theoretical results [38–40]. We calculate also crystal field-dependent behaviors of dynamic M, CF, and RM and present in figures 5(a)–(c). Figure 5(a) illustrates system does not give any phase transition and is in a paramagnetic phase. Therefore, HL is symmetrical and this fact is clearly shown in figure 4. The triple hysteresis behavior is observed in the HL of the system at $-0.4 < d < 1.5$. In figures 5(b) and (c), by increasing the crystal field value, both CF and RM first decrease smoothly and then increase smoothly again. Figure 6 shows the temperature-dependent behavior of HL. We can see that from this figure, there is no

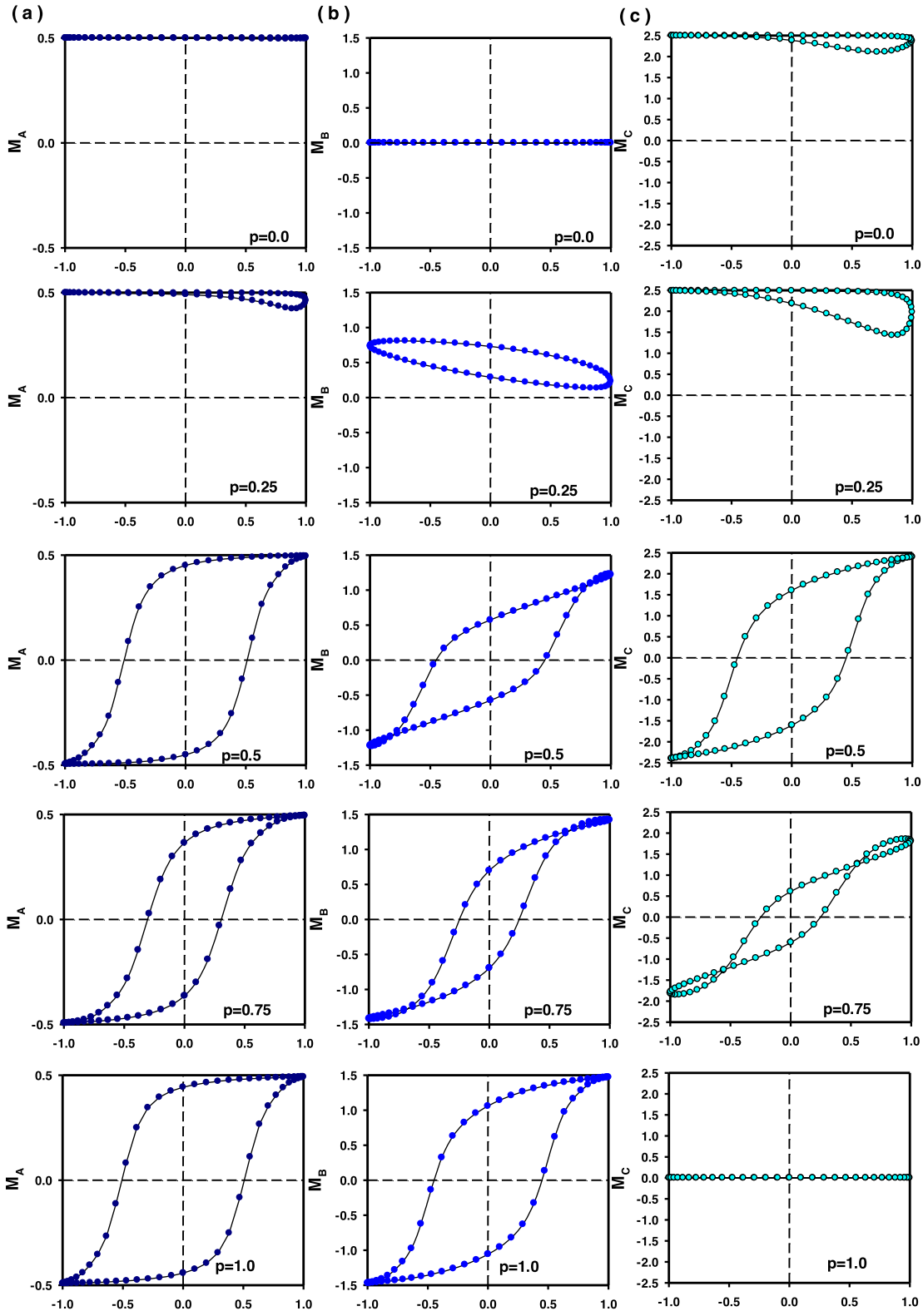

Figure 8. The dynamic magnetic hysteresis loops of the system with varying p from 0.0 to 1.0 at $T = 1.0$, $J_{AC} = 1.0$, $d = 1.0$, $h_0 = 1.0$, and $\omega = 0.06\pi$ (a) M_A (b) M_B and (c) M_C.

HL in the system for very small temperatures, namely 0.2. By increasing the temperature, one single narrow HL appears and then it evolves into a symmetrical rectangular shape at $T = 0.76$. If the temperature value is further increased, the HL begins to take on a thin symmetrical form and is seen as triple HL in this system. After $T \geqslant 1.5$, the system evolves into a symmetrical ellipsis. Additionally, our findings quantitatively compatible with a number of theoretical findings [39, 40] as well as experimental observations on ultrathin epitaxial Fe/GaAs and Fe/InAs(001) [41], Fe thin films [42], Co films on Cu (001) [43]. In figure 7, the dynamic M, CF, and RM are calculated with the same parameters as those used in figure 6. Figure 7(a) shows the first-order phase transitions

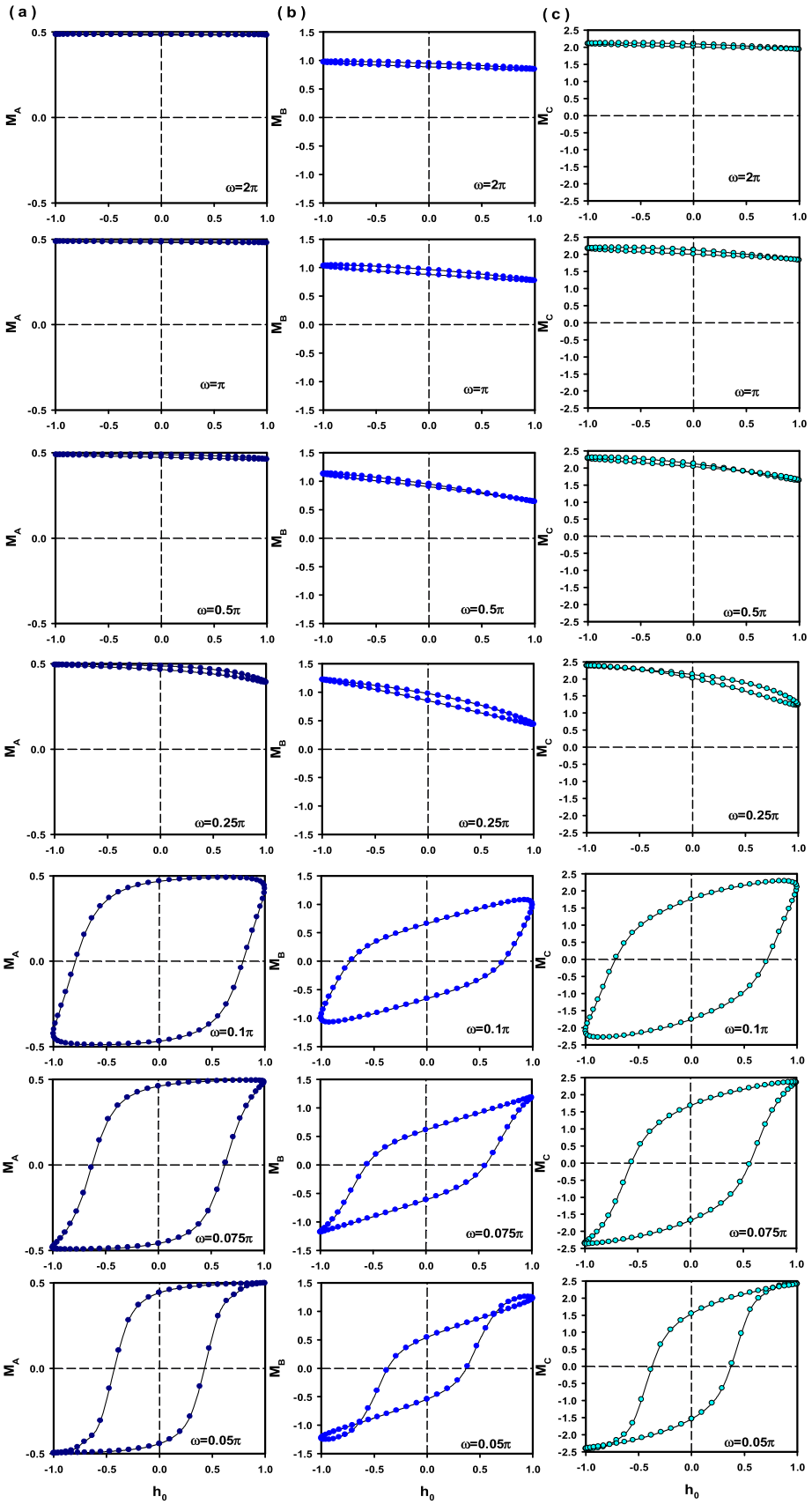

Figure 9. The dynamic magnetic hysteresis loops of the system with varying ω from 0.05π to 2.0π at $T = 1.0$, $J_{AC} = 1.0$, $d = 1.0$, $h_0 = 1.0$, and $p = 0.5$ (a) M_A (b) M_B and (c) M_C.

from the ferrimagnetic phase to paramagnetic phase at $T = 0.76$. From figures 7(b) and (c) we observe that both *CF* and *RM* first decrease smoothly and then increase smoothly. The concentration ratio p dependence of the HL is investigated and the results obtained are presented in figure 8. There is no HL in the system for

$0 < p < 0.28$. While the HL of B sublattice displays triple behavior at $p = 0.5$, the HL of A and C sublattices take the shape of a Lissajous curve. Both B and C sublattices display triple HL for $p = 0.75$ while A sublattice shows one HL. When there is no HL of the C sublattice for $p = 1.0$, A and B sublattices show Lissajous curve. Finally, we present the effect of ω on HL in figure 9 for different values of ω, ranging from 0.05π to 2.0π. The system shows wide HL for a very low value ω. Moreover, the system does not illustrate HL for frequency values greater than 0.25π. We observed similar results in some theoretical studies [44, 45] and some experimental results, namely [46, 47].

4. Summary and conclusion

In summary, the mean-field approximation and Glauber-type stochastic dynamics have been used to study the dynamic hysteresis characteristics of mixed spins-$(1/2, 3/2, 5/2)$ ternary alloy system with formula $AB_pC_{(1-p)}$. The HL behaviors are examined for different interlayer coupling, crystal-field interactions, temperatures, concentration constants, and frequencies. The HL illustrates symmetrical behavior for $-0.53 \leqslant J_{AC} < 1.20$. For large negative values of d, the system exhibits the elliptical HL shape. As d increases, the number of HL increases from single to triple loops. For very low temperatures, there is no HL in the system. After $T \geqslant 1.5$, the system evolves into a symmetrical ellipsis. There is no HL in the system for low p, namely $0 < p < 0.28$. The system displays wide HL for a very low ω value. We also investigate the variation of the coercive field and remanent magnetization with the reduced temperature and the interlayer coupling constant. We observe that our results are in good agreement with some theoretical and experimental results. Our findings demonstrate that the Hamiltonian parameters have a delicate influence on the dynamic hysteresis properties' form and quantity.

Finally, we expect that our thorough theoretical exploration will inspire other efforts to empirically investigate the dynamic hysteresis behavior on ternary alloy Ising systems and shed some light on such efforts. We also expect that by employing more precise methods like kinetic Monte Carlo simulations or renormalization-group calculations, theoretical physicists would be inspired to continue their research into the dynamic hysteresis behavior.

Data availability statement

The data cannot be made publicly available upon publication because no suitable repository exists for hosting data in this field of study. The data that support the findings of this study are available upon reasonable request from the authors.

ORCID iDs

M Ertaş https://orcid.org/0000-0001-6054-1157
M Batı https://orcid.org/0000-0003-2304-4869

References

[1] Winkler N, Leuthold J, Lei Y and Wilde G 2012 *J. Mater. Chem.* **22** 16627
[2] Žukovič M and Bobák A 2010 *J. Magn. Magn. Mater.* **322** 2868
[3] Ertaş M. and Batı M. 2023 Dynamic magnetic properties of spin-7/2 multilayer Ising system in an oscillating magnetic field *Phase Transitions* **96** 246–257
[4] Buendía G and Villarroel J 2007 *J. Magn. Magn. Mater.* **310** e495
[5] Motlagh H N and Rezaei G 2017 *J. Alloys Compd.* **711** 677
[6] Hashimoto K and Ohkoshi H 1999 *Phys. Eng. Sci.* **357** 2977
[7] Hu H, Xin Z and Liu W 2006 *Phys. Lett.* A **357** 388
[8] Abubrig O, Bobák A, Horváth D and Jaščur M 2002 *J. Czech Phys.* **52** 131
[9] Yigit A and Albayrak E 2013 *Chin. Phys.* B **22** 100508
[10] Buendía G M and Villarroel J E 2007 *J. Magn. Magn. Mater.* **310** e495
[11] Mert G 2014 *J. Magn. Magn. Mater.* **363** 224
[12] Vatansever E, Yüksel Y and Alloys J 2016 *Comp.* **689** 446
[13] Alzate-Cardona J D, Restrepo-Parra E and Acosta-Medina C D 2018 *Mater. Chem. Phys.* **213** 362e367
[14] Batı M and Ertaş M 2021 *Eur. Phys. J. Plus* **136** 20
[15] Batı M and Ertaş M 2021 *Physica* A **573** 125938
[16] Yüksel Y 2013 *Phys. Lett.* A **377** 2494
[17] Batı M and Ertaş M *Mater. Today Commun., Under Review*
[18] Chakrabarti B K and Acharyya M 1999 *Rev. Mod. Phys.* **71** 847
[19] Tomé T and de Oliveira M J 1990 *Phys. Rev.* A **41** 4251

[20] Yüksel Y, Vatansever E and Polat H 2012 *J. Phys. Cond. Matt.* **24** 436004
[21] Acharyya M 1998 *Phys. Rev.* E **58** 179
[22] Lo W S and Pelcovits R A 1990 *Phys. Rev.* A **42** 7471
[23] Lee W Y, Samed A, Moore T A, Bland J A C and Choi B C 2000 *J. Appl. Phys.* **87** 6600
[24] Robb D T, Xu Y H, Hellwig O, McCord J, Berger A, Novotny M A and Rikvold P A 2008 *Phys. Rev. B* **78** 134422
[25] dos Reis D C, França E L T, de Paula V G, dos Santos A O, Coelho A A, Cardoso L P and da Silva L M 2017 *J. Magn. Magn. Mater.* **424** 84
[26] Li K *et al* 2014 *Solid State Commun.* **192** 89
[27] Prester M, Živković I, Drobac D, Šurija V, Pajić D and Berger H 2011 *Phys. Rev. B* **84** 064441
[28] Cerruti B and Zapperi S 2007 *Phys. Rev.*B **75** 064416
[29] Landi G T and Santos A D 2012 *J. Appl. Phys.* **111** 07D121
[30] Ourai B, Titov S V, El Mrabti H and Kalmykov Y P 2013 *J. Appl. Phys.* **113** 053903
[31] Dimitrov D and Veysin G M 1994 *Phys. Rev.* B **50** 3077
[32] Aktaş B O, Akıncı Ü and Polat H 2014 *Phys. Rev. E* **90** 012129
[33] Ertaş M, Batı M and Temizer Ü 2018 *Chin. J. Phys.* **56** 807
[34] Mijatovic S, Graovac S, Spasojevic D and Tadic B 2022 *Physica E* **142** 115319
[35] Spasojevic D, Mijatovic S and Janicevic S 2023 *J. Stat. Mech: Theory Exp.* **2023** 033210
[36] Cerruti B, Durin G and Zapperi S 2009 *Phys. Rev. B* **79** 134429
[37] Bertotti G 1998 *Hysteresis in Magnetism* (New York: Academic)
[38] Dalven R 1990 *Introduction to Applied Solid State Physics* (New York: Plenum Press)
[39] Batı M and Ertaş M 2016 *J. Supercond. Nov. Magn.* **29** 2835
[40] Ertaş M and Temizer Ü 2022 *Eur. J. Phys. Plus* **137** 1202
[41] Moore T A, Rothman J, Xu Y B and Bland J A C 2001 *J. Appl. Phys.* **89** 7018
[42] Suen J S and Erskine J L 1997 *Phys. Rev. Lett.* **78** 3567
[43] Suen J S, Lee M H, Teeter G and Erskine J L 1999 *Phys. Rev.* B **59** 4249
[44] Kantar E and Ertaş M 2015 *J. Supercond. Nov. Magn.* **28** 2529
[45] Batı M and Ertaş M 2017 *Physica* B **513** 40
[46] Fleace C T, Morjan I, Alexandrescu R, Dumitrache F, Soare I, Gavrilla-Florescu I, Normand F I and Derory A 2009 *Appl. Surf. Sci.* **255** 5386
[47] Skumryev V, Stoyanov S, Zhang Y, Hadjipanayis G, Givord D and Nogues J 2003 *Nature* **423** 850